Numerical solution of coupled nonlinear Klein-Gordon equations on unbounded domains

Yinong Tai, Hongwei Li ⓞ,[*] Zhaojie Zhou, and Ziwen Jiang

School of Mathematics and Statistics, Shandong Normal University, Jinan 250358, People's Republic of China

The numerical solution of coupled nonlinear Klein-Gordon equations on unbounded domains is considered by applying the artificial boundary method. Based on the unified approach to overcome the coupled nonlinearity, local artificial boundary conditions are designed on the introduced artificial boundaries. The original problem is reduced to an initial boundary value problem on a bounded domain, which can be efficiently solved by the finite difference method. Some numerical examples are provided to verify the accuracy and effectiveness of the proposed method.

I. INTRODUCTION

The coupled nonlinear Klein-Gordon equations on unbounded domain have considerable applications in the field of mathematical physics, such as hydrodynamics, plasma physics, optical fiber, solid physics, chemical kinematics, chemical physics, and geochemistry [1,2]. A particularly important application of these equations is in the area of relativistic quantum mechanics. In this paper, we consider the numerical solution of the following coupled nonlinear Klein-Gordon equations (CNLKGEs) with cubic nonlinearity:

$$\psi_{tt}(\mathbf{x}, t) - a^2 \nabla^2 \psi(\mathbf{x}, t) + f(\psi, \phi) = 0, \tag{1}$$

$$\phi_{tt}(\mathbf{x}, t) - a^2 \nabla^2 \phi(\mathbf{x}, t) + g(\psi, \phi) = 0, \tag{2}$$

$$\psi(\mathbf{x}, 0) = \psi^{(0)}(\mathbf{x}), \quad \psi_t(\mathbf{x}, 0) = \psi^{(1)}(\mathbf{x}), \tag{3}$$

$$\phi(\mathbf{x}, 0) = \phi^{(0)}(\mathbf{x}), \quad \phi_t(\mathbf{x}, 0) = \phi^{(1)}(\mathbf{x}), \tag{4}$$

where $(\mathbf{x}, t) \in \mathbb{R}^d \times (0, T]$, and ∇ represents a d-dimensional gradient operator with $d = 1, 2$. The coupled nonlinear functions $f(\psi, \phi)$ and $g(\psi, \phi)$ are given as

$$f(\psi, \phi) = a_1 \psi + b_1 \psi^3 + c_1 \psi \phi^2,$$
$$g(\psi, \phi) = a_2 \phi + b_2 \phi^3 + c_2 \phi \psi^2.$$

These equations model the motion of charged mesons in an electromagnetic field. The real-valued functions $\psi(\mathbf{x}, t)$ and $\phi(\mathbf{x}, t)$ are scalar fields of charged mesons with masses $a_1^{1/2}$ and $a_2^{1/2}$. b_i and c_i $(i = 1, 2)$ represent the interaction constants of two charged mesons, and they are both positive or negative. The CNLKGEs satisfy the following energy conservation in the whole space:

$$E(t) := \int_{\mathbb{R}^d} \left\{ \frac{c_2}{c_1} [(\psi_t)^2 + a^2 |\nabla \psi|^2] + (\phi_t)^2 \right.$$
$$\left. + a^2 |\nabla \phi|^2 + G(\psi, \phi) \right\} d\mathbf{x} = E(0), \tag{5}$$

where

$$G(\psi, \phi) = \frac{c_2}{c_1} \left(a_1 \psi^2 + \frac{b_1}{2} \psi^4 \right)$$
$$+ a_2 \phi^2 + \frac{b_2}{2} \phi^4 + c_2 (\psi \phi)^2 + M$$

with constant M, and the mass conservation

$$M_{\text{tot}}(t) := \int_{\mathbb{R}^d} (|\psi|^2 + |\phi|^2) d\mathbf{x} \equiv M_{\text{tot}}(0), \quad t \geqslant 0. \tag{6}$$

On the bounded domains, many literatures have studied nonlinear Klein-Gordon equations in numerical aspects, such as finite difference method [3], finite element method [4], and exponential spectral method [5]. For the CNLKGEs, Ji [6] proposed a three-layer conserved nonlinear compact difference scheme with the second-order accuracy in time and the fourth-order accuracy in space, and the discrete conservation law, convergence, and stability of the scheme are discussed. Xu [7] presented a spectral method based on a Gautschi-type integral, which has the second-order convergence rate in time and the spectral convergence rate in space, and estimated the error of the proposed method. Dong designed a scheme for N-coupled nonlinear Klein-Gordon equations based on the trigonometric polynomials, and the accuracy and stability are presented [8].

However, few works studied the numerical solution for the CNLKGEs on unbounded domains, due to the unboundedness of the physical domain. One popular and efficient approach to overcome the unboundedness is the artificial boundary method, in which the idea is to truncate the unbounded domain into the bounded computational domain by developing the appropriate artificial or absorbing boundary conditions (ABCs) on the introduced artificial boundaries. Generally speaking, the ABCs can be divided into global [9–17] and local [18,19] ABCs. The global ABCs are easy to design and the algorithm is robust, but the computation is large and the geometry of the computational domain is strict. Although the precision of the local ABCs is generally inferior to the global ABCs, the algorithm and computation of the local ABCs are simple and small, respectively. Thus, the local ABCs have succeeded to

---

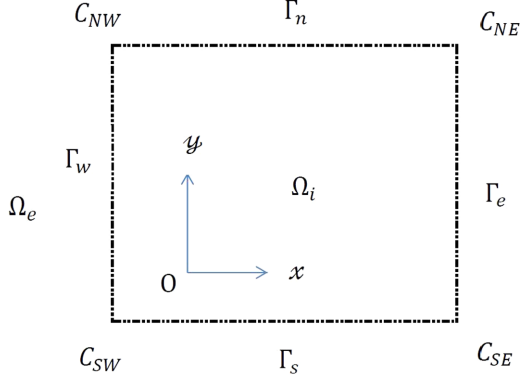*Corresponding author: hwli@sdnu.edu.cn

FIG. 1. Settings of unbounded domain.

solve many partial differential equations on unbounded domain, such as the wave equation [18] and heat equation [20].

Another difficulty to design the local ABCs for the CN-LKGEs is the nonlinearity of the coupled equations. The unified approach, stemming from the well-known operator splitting method, is developed to construct the local ABCs for the nonlinear partial differential equations, including the nonlinear Schrödinger equation and nonlinear wave equation [21–24]. Han and Zhang [25–27] proposed the local ABCs of a nonlinear Klein-Gordon equation by using the idea of operator splitting, and extended this idea from one dimension to two dimensions and for a two-level Schrödinger equation. Zhou and Cheng [28] adopted the method of operator splitting to solve the coupled nonlinear Schrödinger equations, in which the linear subproblem is introduced into the artificial boundary, and the nonlinear subproblem is an ordinary differential equation that can be solved accurately. Li and Guo [29,30] proposed the local ABCs of the coupled nonlinear Schrödinger equation by using the idea of operator splitting, and introduced the auxiliary function to analyze the stability of the reduced initial boundary value problem.

The organization of this paper is as follows. In Sec. II, based on ideas of the artificial boundary method and operator splitting approach, the local ABCs for the two-dimensional CNLKGEs are derived on the introduced artificial boundaries, and an initial boundary value problem (IBVP) is obtained. The finite difference scheme for the reduced IBVP is established in Sec. III. In Sec. IV, some numerical examples are presented to verify the validity and convergence of the proposed scheme. Some concluding remarks are given in Sec. V.

II. DESIGN OF ABCs

In this section, for the sake of simplicity, we focus on the derivation of local ABCs for two-dimensional

TABLE II. An exact solution and numerical solution on the artificial boundary point for different times.

	$T = 0.5$	$T = 0.6$	$T = 0.7$	$T = 0.8$	$T = 0.9$	$T = 1$
Exact	0.01197	0.03254	0.08829	0.23631	0.57688	0.89441
Numerical	0.01193	0.03242	0.08795	0.23537	0.57448	0.89212

CNLKGEs by adopting the idea of the well-known operator splitting method. As shown in Fig. 1, the unbounded domain was divided into two parts, including interior domain Ω_i and exterior domain $\Omega_e = \mathbb{R}^2 \backslash \bar{\Omega}_i$, by the east-, south-, west- and north-artificial boundaries $\Gamma = \{\Gamma_e, \Gamma_s, \Gamma_w, \Gamma_n\}$. $\{C_{SE}, C_{SW}, C_{NW}, C_{NE}\}$ represent the corresponding corners, respectively, where

$$\Omega_i = \{(x, y)|x_w < x < x_e, y_s < y < y_n\},$$

$$\Gamma_e = \{(x, y)|x = x_e, y_s < y < y_n\},$$

$$\Gamma_s = \{(x, y)|y = y_s, x_w < x < x_e\},$$

$$\Gamma_w = \{(x, y)|x = x_w, y_s < y < y_n\},$$

$$\Gamma_n = \{(x, y)|y = y_n, x_w < x < x_e\}.$$

Introducing some auxiliary variables

$$\Psi = [\psi, \phi]^T, \quad \Phi = [\Psi, \Psi_t]^T,$$

$$P(\Psi) = -[f(\psi, \phi), g(\psi, \phi)]^T.$$

For the sake of simplicity, we consider the original problem in the following operator form:

$$\Phi_t \equiv (\Psi_t, \Psi_{tt})^T = \mathcal{L}\Phi + \mathcal{N}\Phi, \tag{7}$$

with

$$\mathcal{L}\Phi = \begin{pmatrix} \Psi_t \\ a^2(\Psi_{xx} + \Psi_{yy}) \end{pmatrix} \quad \text{and} \quad \mathcal{N}\Phi := \begin{pmatrix} 0 \\ P(\Psi) \end{pmatrix},$$

where $\mathcal{L}$ and $\mathcal{N}$ represent the kinetic energy and potential energy operator. The operator splitting method means that the wave propagation performs the action of kinetic energy step and potential energy step, respectively, in a small time size τ. In a small time interval, we have the following equation by using the operator splitting method:

$$\Phi(x, y, t + \tau) \approx e^{(\mathcal{L}+\mathcal{N})\tau}\Phi(x, y, t). \tag{8}$$

In order to design the local ABCs, the idea is to approximate linear operator $\mathcal{L}$ by the operator $\widetilde{\mathcal{L}}$ and obtain the one-way equation.

TABLE I. The L_1, L_∞, and L_2 error and the corresponding convergence order with the parameters $a = \sqrt{101}$, $a_1 = 1$, $b_1 = -2$, $c_1 = -1$, $a_2 = 1$, $b_2 = -3$, $c_2 = -1$, $v = 10$ at time $T = 0.5$.

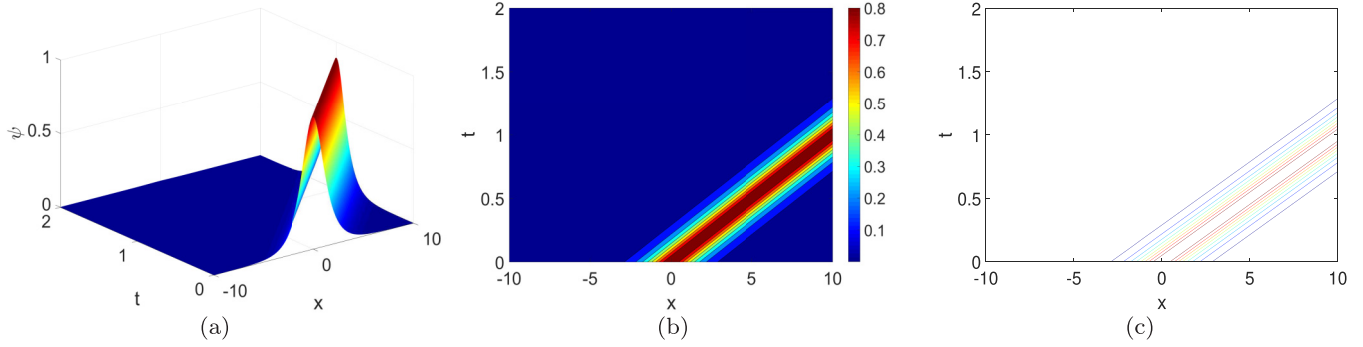| Mesh	L_1-E	Order	L_∞-E	Order	L_2-E	Order
$h = \frac{1}{10}$	2.100×10^{-3}		2.520×10^{-2}		2.920×10^{-2}	
$h = \frac{1}{20}$	5.085×10^{-4}	2.046	5.800×10^{-3}	2.119	6.300×10^{-3}	2.213
$h = \frac{1}{40}$	1.256×10^{-4}	2.018	1.400×10^{-3}	2.050	1.500×10^{-3}	2.071
$h = \frac{1}{80}$	3.131×10^{-5}	2.004	3.556×10^{-4}	1.964	3.775×10^{-4}	1.991

FIG. 2. The evolution of $|\psi|$ for $a = \sqrt{101}$, $a_1 = 1$, $b_1 = -2$, $c_1 = -1$, $a_2 = 1$, $b_2 = -3$, $c_2 = -1$, $v = 10$, $x_w = -10$, $x_e = 10$, $h = 1/40$, $\tau = h^2$ in Example 1.

Higdon [18] approximated the dispersion relation with high precision, and obtained the regular ABCs on the east boundary Γ_e,

$$\prod_{l=1}^{p}(\cos\theta_l \partial_t + a\partial_x)\Psi = 0,$$

where p is an integer and $\pm\theta_l$ ($l = 1, 2, \ldots, p$) are the angles between the wave incident direction and the normal direction of the boundary. The east ABCs are composed of p factor $\cos\theta_l \partial_t + a\partial_x$. The parameter p is selected as $p = 2$ in this paper, and the ABCs of the linear wave equations on the east boundary are as follows:

$$\cos\theta_1 \cos\theta_2 \psi_{tt} + a(\cos\theta_1 + \cos\theta_2)\psi_{xt} + a^2 \psi_{xx} = 0, \tag{9}$$

$$\cos\theta_1 \cos\theta_2 \phi_{tt} + a(\cos\theta_1 + \cos\theta_2)\phi_{xt} + a^2 \phi_{xx} = 0. \tag{10}$$

Then, we derive the approximate linear operator $\widetilde{\mathcal{L}}$. Setting

$$Q = \begin{pmatrix} 1 & 0 & 0 & 0 \\ a(\cos\theta_1 + \cos\theta_2)\partial_x & 0 & \cos\theta_1 \cos\theta_2 & 0 \\ 0 & 1 & 0 & 0 \\ 0 & a(\cos\theta_1 + \cos\theta_2)\partial_x & 0 & \cos\theta_1 \cos\theta_2 \end{pmatrix},$$

Eqs. (9) and (10) can be equivalently rewritten by

$$\Phi_t = Q^{-1}\begin{pmatrix} \psi_t \\ -a^2 \psi_{xx} \\ \phi_t \\ -a^2 \phi_{xx} \end{pmatrix} \equiv \widetilde{\mathcal{L}}\Phi. \tag{11}$$

By considering the linear subproblem in operator form, the approximate operator $\widetilde{\mathcal{L}}$ can be obtained:

$$\mathcal{L} \approx \widetilde{\mathcal{L}} := Q^{-1}\begin{pmatrix} 0 & 0 & 1 & 0 \\ -a^2\partial_x^2 & 0 & 0 & 0 \\ 0 & 0 & 0 & 1 \\ 0 & -a^2\partial_x^2 & 0 & 0 \end{pmatrix}. \tag{12}$$
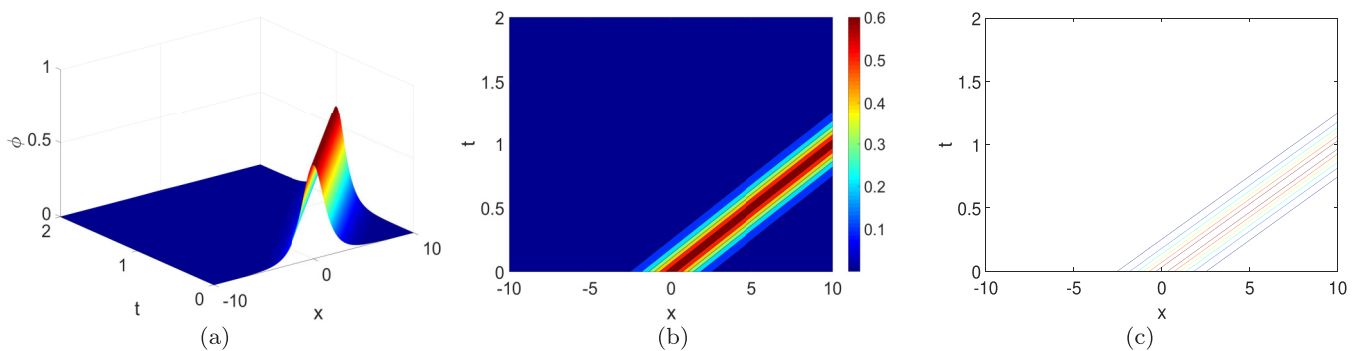

FIG. 3. The evolution of $|\phi|$ for $a = \sqrt{101}$, $a_1 = 1$, $b_1 = -2$, $c_1 = -1$, $a_2 = 1$, $b_2 = -3$, $c_2 = -1$, $v = 10$, $x_w = -10$, $x_e = 10$, $h = 1/40$, $\tau = h^2$ in Example 1.
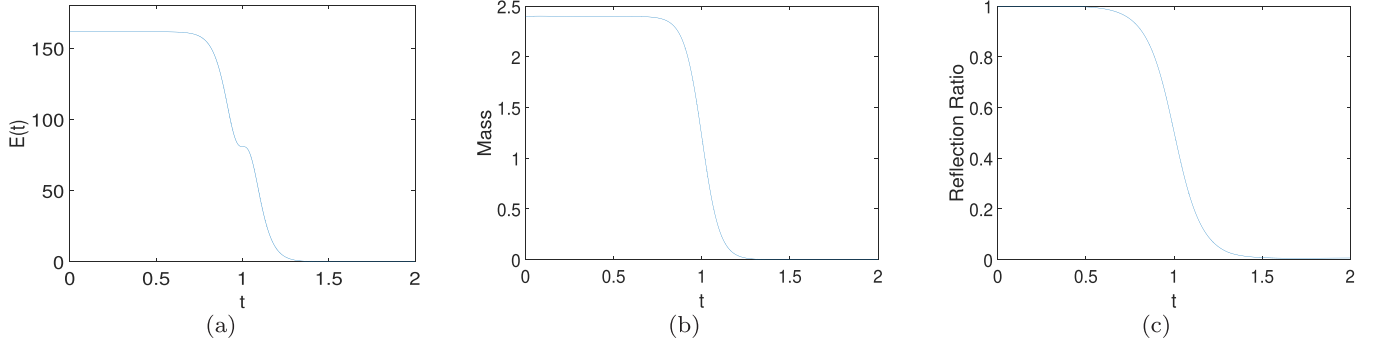
FIG. 4. The energy, mass, and reflection ratios for the parameters $a = \sqrt{101}$, $a_1 = 1$, $b_1 = -2$, $c_1 = -1$, $a_2 = 1$, $b_2 = -3$, $c_2 = -1$, $v = 10$, $x_w = -10$, $x_e = 10$, $h = 1/40$, $\tau = h^2$ in Example 1.

There are four boundaries in the two-dimensional case. Each boundary of the coupled equations requires two ABCs. Below, we only give the ABCs of linear subproblem ψ in the west, north, and south directions in turn.

$$\cos\theta_1 \cos\theta_2 \psi_{tt} - a(\cos\theta_1 + \cos\theta_2)\psi_{xt} + a^2\psi_{xx} = 0, \quad (13)$$

$$\cos\theta_1 \cos\theta_2 \psi_{tt} + a(\cos\theta_1 + \cos\theta_2)\psi_{yt} + a^2\psi_{yy} = 0, \quad (14)$$

$$\cos\theta_1 \cos\theta_2 \psi_{tt} - a(\cos\theta_1 + \cos\theta_2)\psi_{yt} + a^2\psi_{yy} = 0. \quad (15)$$

Next we construct the local ABCs of the CNLKGEs. Since the designed process of all the ABCs on the artificial boundaries is similar, we only give the derivation of the ABCs on the east boundary. Now we have derived the approximation linear operator $\widetilde{\mathcal{L}}$ and brought it into the one-way equation

$$\Phi_t = \widetilde{\mathcal{L}}\Phi + \mathcal{N}\Phi. \quad (16)$$

By multiplying Eq. (16) by operator Q, we can obtain the ABCs of the coupled nonlinear equations on the east boundary:

$$\cos\theta_1 \cos\theta_2 \psi_{tt} + a(\cos\theta_1 + \cos\theta_2)\psi_{xt} + a^2\psi_{xx}$$
$$- \cos\theta_1 \cos\theta_2 f(\psi, \phi) = 0, \quad (17)$$

$$\cos\theta_1 \cos\theta_2 \phi_{tt} + a(\cos\theta_1 + \cos\theta_2)\phi_{xt} + a^2\phi_{xx}$$
$$- \cos\theta_1 \cos\theta_2 g(\psi, \phi) = 0. \quad (18)$$

By repeating the above process, we can get the following local ABCs of the CNLKGEs on the west, north, and south boundaries in turn:

$$\cos\theta_1 \cos\theta_2 \psi_{tt} - a(\cos\theta_1 + \cos\theta_2)\psi_{xt} + a^2\psi_{xx}$$
$$- \cos\theta_1 \cos\theta_2 f(\psi, \phi) = 0, \quad (19)$$

$$\cos\theta_1 \cos\theta_2 \psi_{tt} + a(\cos\theta_1 + \cos\theta_2)\psi_{yt} + a^2\psi_{yy}$$
$$- \cos\theta_1 \cos\theta_2 f(\psi, \phi) = 0, \quad (20)$$

$$\cos\theta_1 \cos\theta_2 \psi_{tt} - a(\cos\theta_1 + \cos\theta_2)\psi_{yt} + a^2\psi_{yy}$$
$$- \cos\theta_1 \cos\theta_2 f(\psi, \phi) = 0, \quad (21)$$

$$\cos\theta_1 \cos\theta_2 \phi_{tt} - a(\cos\theta_1 + \cos\theta_2)\phi_{xt} + a^2\phi_{xx}$$
$$- \cos\theta_1 \cos\theta_2 g(\psi, \phi) = 0, \quad (22)$$

$$\cos\theta_1 \cos\theta_2 \phi_{tt} + a(\cos\theta_1 + \cos\theta_2)\phi_{yt} + a^2\phi_{yy}$$
$$- \cos\theta_1 \cos\theta_2 g(\psi, \phi) = 0, \quad (23)$$

$$\cos\theta_1 \cos\theta_2 \phi_{tt} - a(\cos\theta_1 + \cos\theta_2)\phi_{yt} + a^2\phi_{yy}$$
$$- \cos\theta_1 \cos\theta_2 g(\psi, \phi) = 0. \quad (24)$$

Coupling those local ABCs (17)–(24) with the CN-LKGEs (1)–(4), the original problem on unbounded domain was reduced to an IBVP on a bounded domain, which can be solved by applying the finite difference method efficiently.
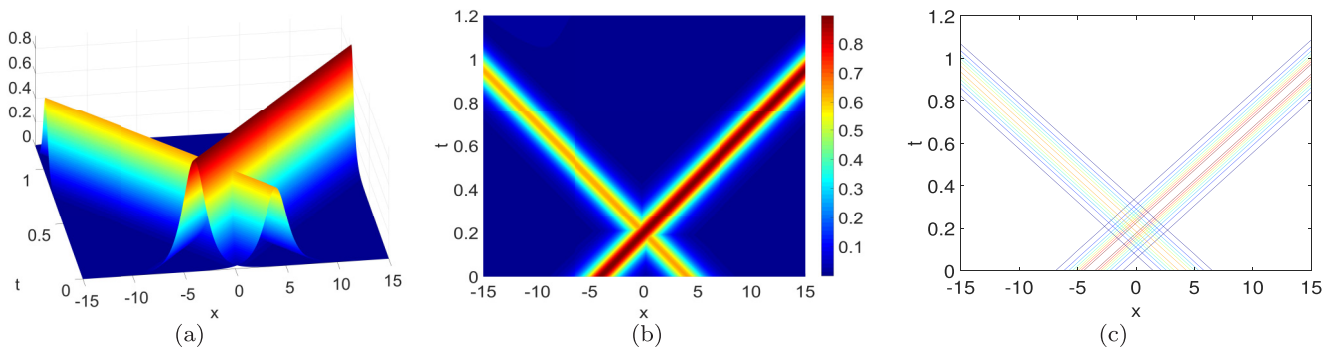

FIG. 5. The evolution of $|\psi|$ and $|\phi|$ for $a = \sqrt{401}$, $a_1 = 1$, $b_1 = -2$, $c_1 = -1$, $a_2 = 1$, $b_2 = -3$, $c_2 = -1$, $v = 20$, $x_0 = 4$, $h = 1/40$, $\tau = h^2$ in Example 2.
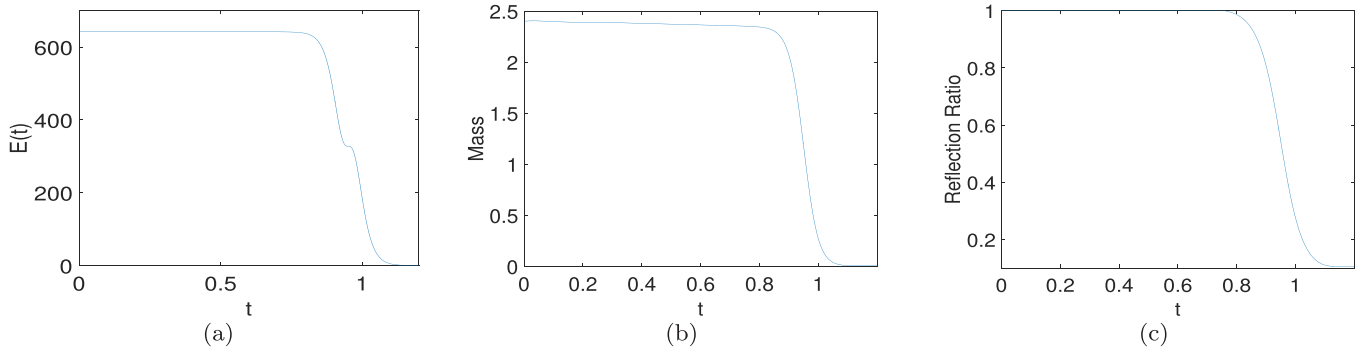
(a) (b) (c)

FIG. 6. The energy, mass, and reflection ratios for the parameters $a = \sqrt{401}$, $a_1 = 1$, $b_1 = -2$, $c_1 = -1$, $a_2 = 1$, $b_2 = -3$, $c_2 = -1$, $v = 20$, $x_0 = 4$, $h = 1/40$, $\tau = h^2$ in Example 2.

Remark 1. Although this paper only presents the local ABCs in two dimensions for CNLKGEs, in fact, the local ABCs can be easily extended to CNLKGEs in one dimension.

III. DISCRETIZATION

In this section, we consider the discretization of the reduced IBVPs (1)–(4) and (17)–(24) on a bounded region of a rectangle $\Omega = [x_w, x_e] \times [y_s, y_n] \times [0, T]$, and set $h_x =$ $(x_e - x_w)/J$, $h_y = (y_n - y_s)/K$, and $\tau = T/N$ for the grid size in space and time. For simplicity, the following notations will be used hereafter:

$$D_\tau^+ u_{j,k}^n = \frac{u_{j,k}^{n+1} - u_{j,k}^n}{\tau}, \quad D_\tau^- u_{j,k}^n = \frac{u_{j,k}^n - u_{j,k}^{n-1}}{\tau},$$

$$D_{h_x}^+ u_{j,k}^n = \frac{u_{j+1,k}^n - u_{j,k}^n}{h_x}, \quad D_{h_x}^- u_{j,k}^n = \frac{u_{j,k}^n - u_{j-1,k}^n}{h_x},$$
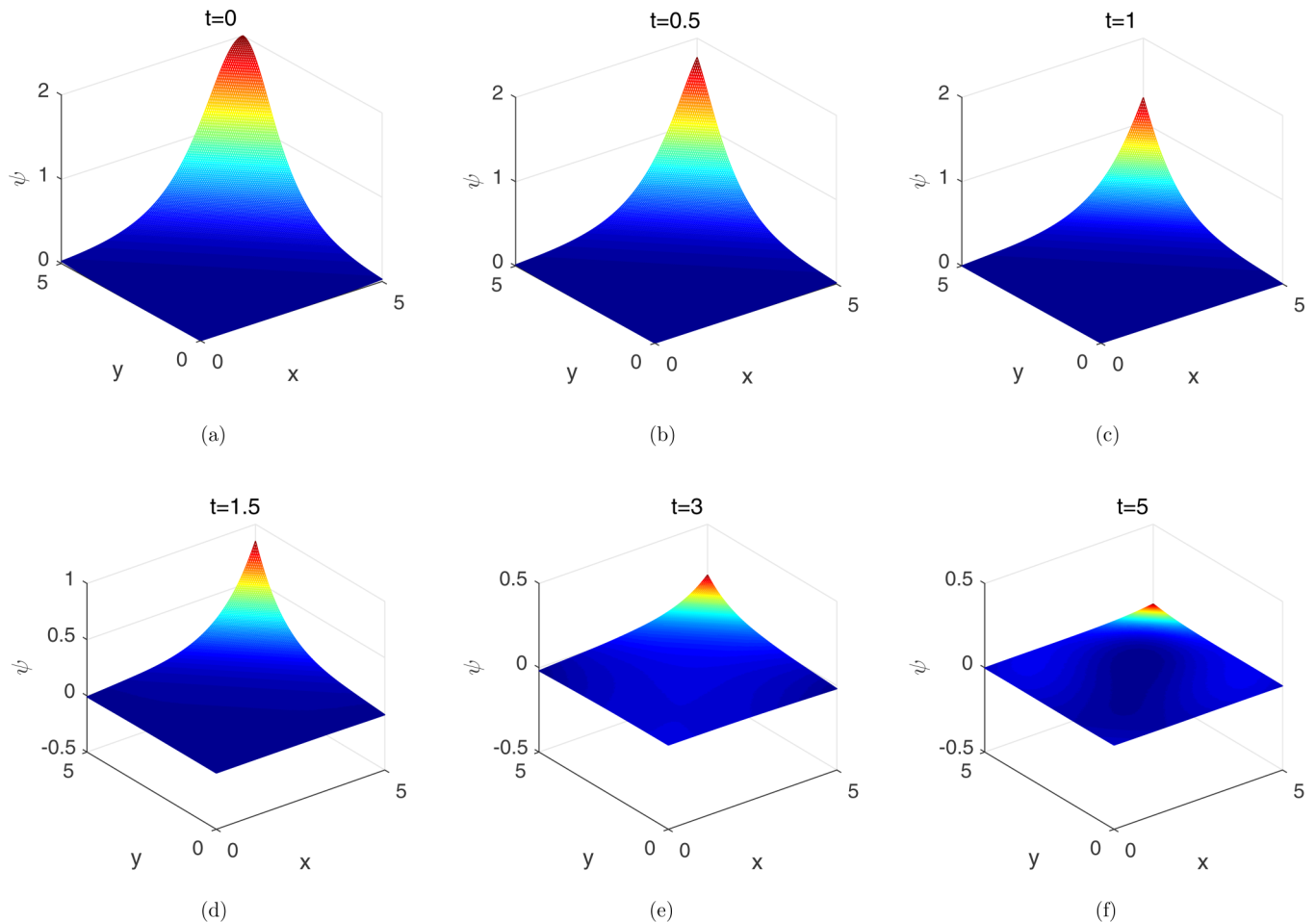

(a) (b) (c)

(d) (e) (f)

FIG. 7. The evolution of ψ for $a = 1$, $a_1 = 1$, $b_1 = -1$, $c_0 = 10$, $c_1 = 1$, $a_2 = 1$, $b_2 = -2$, $c_2 = 0.5$, $v = 1$, $h = 1/32$, $\tau = h^2$ in Example 3.

FIG. 8. The evolution of ψ for $a = 1$, $a_1 = 1$, $b_1 = -1$, $c_0 = 10$, $c_1 = 1$, $a_2 = 1$, $b_2 = -2$, $c_2 = 0.5$, $v = 1$, $h = 1/32$, $\tau = h^2$ in Example 3.
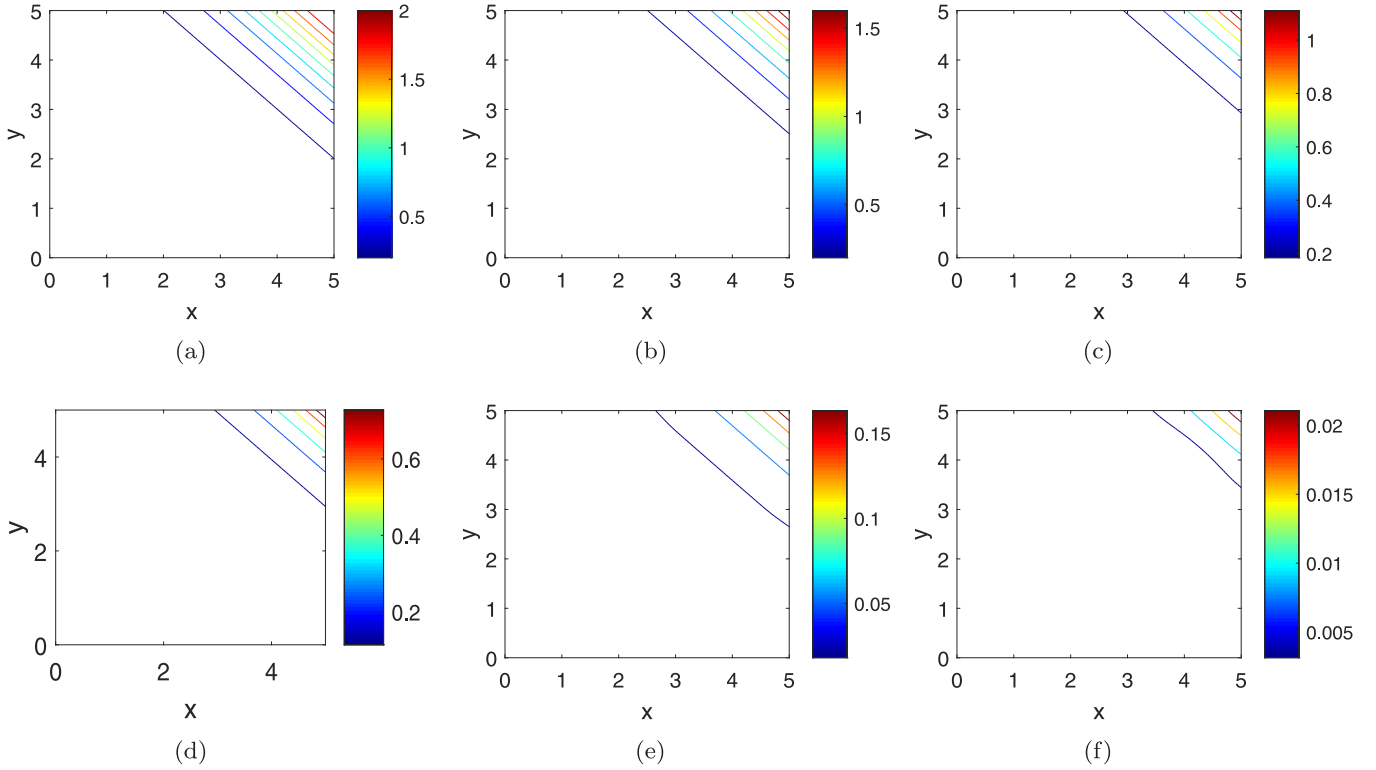
$$D_\tau^0 u_{j,k}^n = \frac{u_{j,k}^{n+1} - u_{j,k}^{n-1}}{2\tau}, \quad D_{h_x}^0 u_{j,k}^n = \frac{u_{j+1,k}^n - u_{j-1,k}^n}{2h_x},$$

$$S_\tau^0 u_{j,k}^n = \frac{u_{j,k}^{n+1} + u_{j,k}^{n-1}}{2}.$$

The IBVPs (1)–(4) and (17)–(24) are discretized on the interior points (x_j, y_k, t_n) of the grid Ω:

$$D_\tau^+ D_\tau^- \psi_{j,k}^n = a^2 \left(D_{h_x}^+ D_{h_x}^- S_\tau^0 \psi_{j,k}^n + D_{h_y}^+ D_{h_y}^- S_\tau^0 \psi_{j,k}^n \right)$$
$$+ f \left(\psi_{j,k}^n, \phi_{j,k}^n \right),$$

$$D_\tau^+ D_\tau^- \phi_{j,k}^n = a^2 \left(D_{h_x}^+ D_{h_x}^- S_\tau^0 \phi_{j,k}^n + D_{h_y}^+ D_{h_y}^- S_\tau^0 \phi_{j,k}^n \right)$$
$$+ g \left(\psi_{j,k}^n, \phi_{j,k}^n \right),$$

where $1 \leqslant j \leqslant J-1$, $1 \leqslant k \leqslant K-1$.

All the local ABCs (17)–(24) and corners are discretized similarly; we only give the discrete finite difference schemes of ABCs on the east boundary and the northeast corner, and the discretization of other boundary conditions can be obtained by analogy. The local ABCs (17) and (18) on the east boundary can be discretized by

$$a(\cos\theta_1 + \cos\theta_2) D_{h_x}^0 D_\tau^0 \psi_{J-1,k}^n + \cos\theta_1 \cos\theta_2 D_\tau^+ D_\tau^- \psi_{J-1,k}^n$$
$$+ a^2 D_{h_x}^+ D_{h_x}^- S_\tau^0 \psi_{J-1,k}^n - \cos\theta_1 \cos\theta_2 f \left(\psi_{J-1,k}^n, \phi_{J-1,k}^n \right) = 0,$$

$$a(\cos\theta_1 + \cos\theta_2) D_{h_x}^0 D_\tau^0 \phi_{J-1,k}^n + \cos\theta_1 \cos\theta_2 D_\tau^+ D_\tau^- \phi_{J-1,k}^n$$
$$+ a^2 D_{h_x}^+ D_{h_x}^- S_\tau^0 \phi_{J-1,k}^n - \cos\theta_1 \cos\theta_2 g \left(\psi_{J-1,k}^n, \phi_{J-1,k}^n \right) = 0,$$

where $1 \leqslant k \leqslant K-1$.

For the corner point (J, K), the discretized scheme is presented as follows:

$$a(\cos\theta_1 + \cos\theta_2) D_{h_x}^0 D_\tau^0 \psi_{J-1,K}^n + \cos\theta_1 \cos\theta_2 D_\tau^+ D_\tau^- \psi_{J-1,K}^n$$
$$+ a^2 D_{h_x}^+ D_{h_x}^- S_\tau^0 \psi_{J-1,K}^n - \cos\theta_1 \cos\theta_2 f \left(\psi_{J-1,K}^n, \phi_{J-1,K}^n \right)$$
$$+ a(\cos\theta_1 + \cos\theta_2) D_{h_y}^0 D_\tau^0 \psi_{J,K-1}^n$$
$$+ \cos\theta_1 \cos\theta_2 D_\tau^+ D_\tau^- \psi_{J,K-1}^n + a^2 D_{h_y}^+ D_{h_y}^- S_\tau^0 \psi_{J,K-1}^n$$
$$- \cos\theta_1 \cos\theta_2 f \left(\psi_{J,K-1}^n, \phi_{J,K-1}^n \right) = 0,$$

$$a(\cos\theta_1 + \cos\theta_2) D_{h_x}^0 D_\tau^0 \phi_{J-1,K}^n + \cos\theta_1 \cos\theta_2 D_\tau^+ D_\tau^- \phi_{J-1,K}^n$$
$$+ a^2 D_{h_x}^+ D_{h_x}^- S_\tau^0 \phi_{J-1,K}^n - \cos\theta_1 \cos\theta_2 g \left(\psi_{J-1,K}^n, \phi_{J-1,K}^n \right)$$
$$+ a(\cos\theta_1 + \cos\theta_2) D_{h_y}^0 D_\tau^0 \phi_{J,K-1}^n$$
$$+ \cos\theta_1 \cos\theta_2 D_\tau^+ D_\tau^- \phi_{J,K-1}^n + a^2 D_{h_y}^+ D_{h_y}^- S_\tau^0 \phi_{J,K-1}^n$$
$$- \cos\theta_1 \cos\theta_2 g \left(\psi_{J,K-1}^n, \phi_{J,K-1}^n \right) = 0.$$

Similarly, the discretization of the reduced IBVPs (1)–(4) and (17)–(24) on the bounded domain is obtained.

IV. NUMERICAL RESULTS

In this section, some numerical examples are given to verify the accuracy and validity of the local ABCs of CNLKGEs, and simulate the evolution of CNLKGEs.
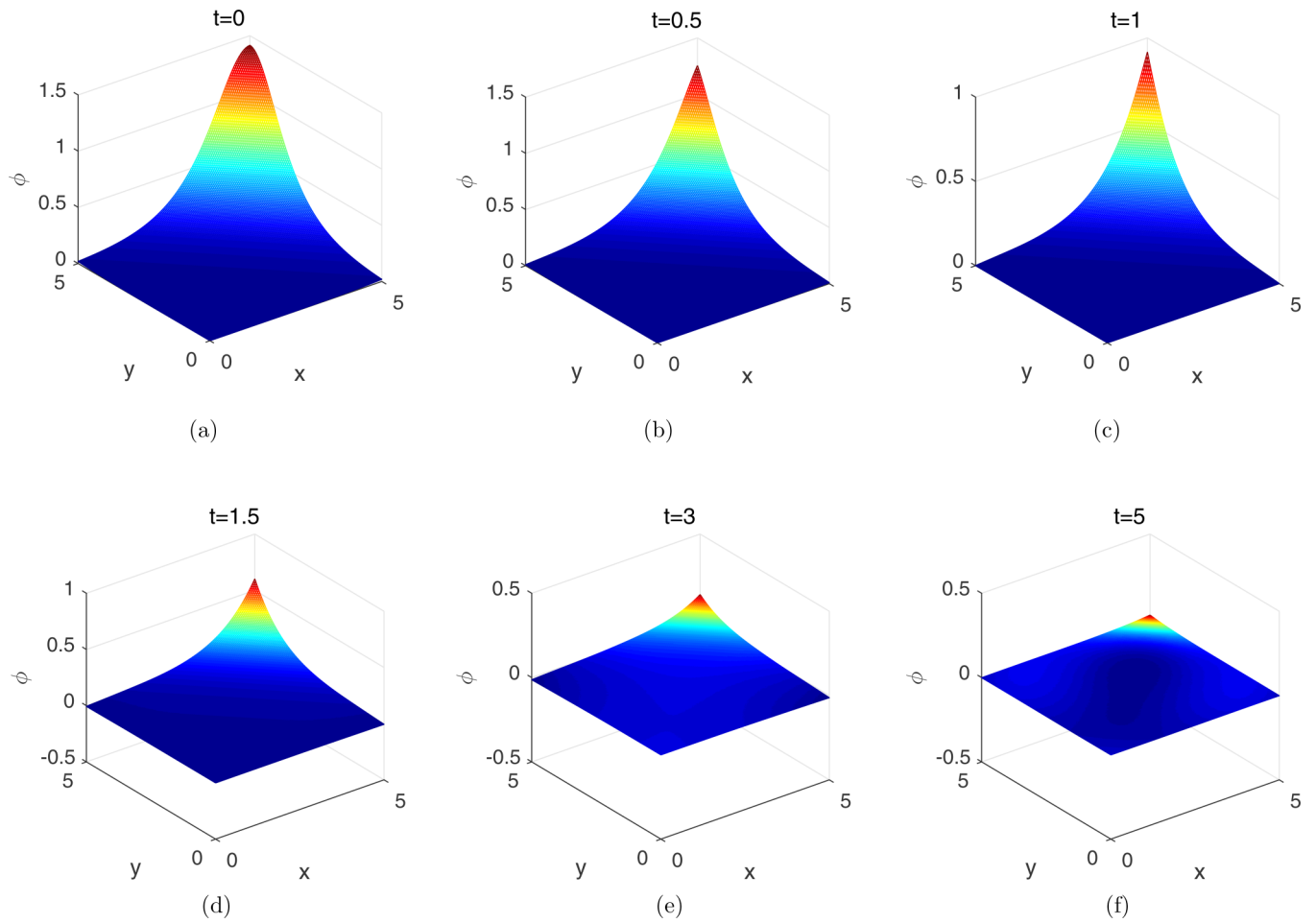
FIG. 9. The evolution of ϕ for $a = 1$, $a_1 = 1$, $b_1 = -1$, $c_1 = 1$, $a_2 = 1$, $b_2 = -2$, $c_2 = 0.5$, $v = 1$, $h = 1/32$, $\tau = h^2$ in Example 3.
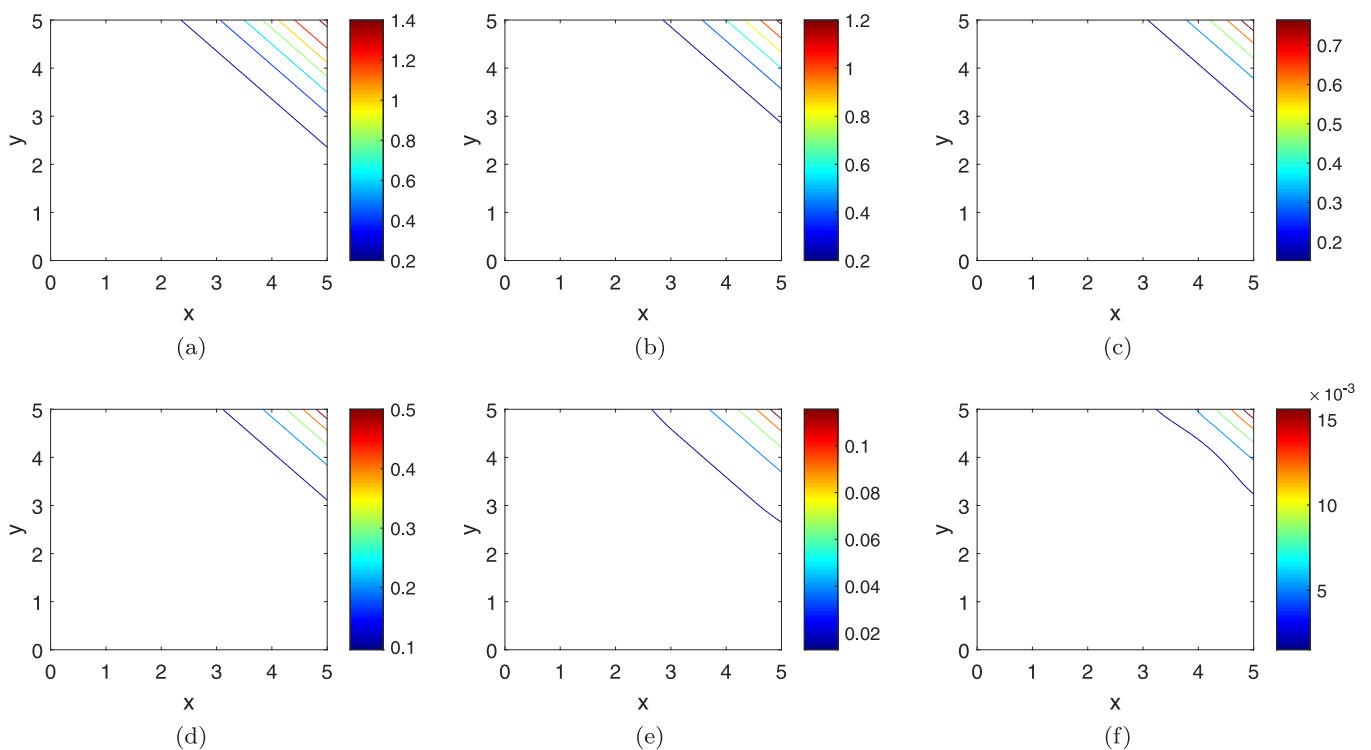
FIG. 10. The evolution of ϕ for $a = 1$, $a_1 = 1$, $b_1 = -1$, $c_1 = 1$, $a_2 = 1$, $b_2 = -2$, $c_2 = 0.5$, $v = 1$, $h = 1/32$, $\tau = h^2$ in Example 3.
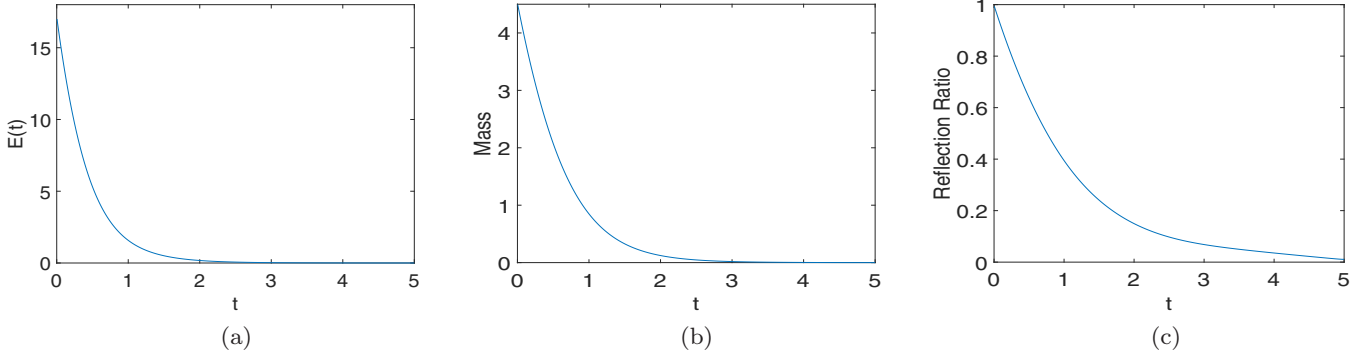
FIG. 11. The energy, mass, and reflection ratios for the parameters $a = 1$, $a_1 = 1$, $b_1 = -1$, $c_1 = 1$, $a_2 = 1$, $b_2 = -2$, $c_2 = 0.5$, $v = 1$, $h = 1/32$, $\tau = h^2$ in Example 3.

A. One-dimensional examples

An exact solution of CNLKGEs in one dimensio is given in [1]:

$$\psi(x, t) = A_1 \text{sech}[B(x - vt)], \quad \phi(x, t) = A_2 \text{sech}[B(x - vt)],$$

where

$$A_1 = \sqrt{\frac{2a_1(c_1 - b_2)}{b_1 b_2 - c_1 c_2}}, \quad A_2 = \sqrt{\frac{2a_2(b_1 - c_2)}{c_1 c_2 - b_1 b_2}},$$

$$B = \sqrt{\frac{-a_1}{v^2 - a^2}}.$$

The L_1, L_2, L_∞ errors are defined to present the accuracy of numerical solution by

$$L_1\text{-E} = \frac{\sum_{j=0}^{J} \sum_{n=0}^{N} \left[\left| \psi_j^n - \psi_{\text{ex}}(x_j, t_n) \right| + \left| \phi_j^n - \phi_{\text{ex}}(x_j, t_n) \right| \right]}{2(J + 1)(N + 1)},$$

$$L_2\text{-E} = \left(\frac{h}{2} \sum_{j=0}^{J} \left[\left| \psi_j^n - \psi_{\text{ex}}(x_j, t_n) \right|^2 + \left| \phi_j^n - \phi_{\text{ex}}(x_j, t_n) \right|^2 \right] \right)^{1/2},$$

$$L_\infty\text{-E} = \frac{\max\left\{ \left| \psi_j^n - \psi_{\text{ex}}(x_j, t_n) \right| \right\} + \max\left\{ \left| \phi_j^n - \phi_{\text{ex}}(x_j, t_n) \right| \right\}}{2},$$

where $\phi_{\text{ex}}(x_j, t_n)$ and $\psi_{\text{ex}}(x_j, t_n)$ are exact solutions of the ϕ and ψ at the point (x_j, t_n), respectively.

Example 1. Assume that the initial conditions are chosen as

$$\psi^{(0)}(x) = A_1 \text{sech}(Bx), \quad \phi^{(0)}(x) = A_2 \text{sech}(Bx),$$

$$\psi^{(1)}(x) = BvA_1 \text{sech}(Bx)\tanh(Bx),$$

$$\phi^{(1)}(x) = BvA_2 \text{sech}(Bx)\tanh(Bx).$$

The numerical solutions were obtained on the computational interval $[-10, 10]$ with the time step $\tau = h^2$. We observe that the work of this local ABC is stable and consists of nearly perfect second-order accuracy from Table I. Figures 2 and 3 show that the artificial boundary is nearly transparent when the wave passes through the right artificial boundary. The energy and mass of CNLKGEs are plotted on the computational interval $[-10, 10]$ in Figs. 4(a) and 4(b). One can easily observe that when the wave moves out of the bounded domain, the energy and mass decay to zero and it shows that the boundary is almost transparent for wave propagation. Table II lists the corresponding numerical solutions and exact solutions at artificial boundary for different times. For the nonlinear Klein-Gordon equation on the unbounded domain, Han and Zhang [25] used the operator splitting method to construct boundary conditions, and we label the first-order operator splitting method as splitting local artificial boundary (SLAB) method. It can be seen from Table III that our method has higher accuracy under the same temporal and spatial steps, but needs longer time. Another important method to test the local ABCs is to show the reflection ratios at t^n defined by [22]

$$r = \sum_{j=0}^{J} \left(\left| \psi_j^n \right| + \left| \phi_j^n \right| \right) \Bigg/ \sum_{j=0}^{J} \left(\left| \psi_j^0 \right| + \left| \phi_j^0 \right| \right).$$

The reflection ratios $r = 1$ and $r = 0$ indicate that the wave is fully reflected back into the calculation area and all across the boundary, respectively. Figure 4(c) shows how the reflection ratio changes over time in one dimension, and

TABLE III. Comparisons of the errors and CPU time of the present scheme and the SLAB method at $T = 1$ with $\tau = 1/5000$.

Mesh	Scheme	L_1-E	L_∞-E	L_2-E	CPU time (s)
$h = \frac{1}{10}$	Present	3.059×10^{-4}	8.100×10^{-3}	2.700×10^{-3}	12.869
	SLAB	4.726×10^{-4}	1.900×10^{-2}	1.670×10^{-2}	11.931
$h = \frac{1}{20}$	Present	1.477×10^{-4}	3.700×10^{-3}	1.500×10^{-3}	40.248
	SLAB	2.088×10^{-4}	9.100×10^{-3}	8.800×10^{-3}	30.716
$h = \frac{1}{40}$	Present	1.167×10^{-4}	2.600×10^{-3}	1.300×10^{-3}	154.584
	SLAB	1.454×10^{-4}	5.300×10^{-3}	5.400×10^{-3}	43.849

TABLE IV. The reference solution and numerical solution on the right artificial boundary point for different times.

	$T = 0.6$	$T = 0.7$	$T = 0.8$	$T = 0.9$	$T = 0.95$	$T = 1$
Exact	0.00161	0.01187	0.08753	0.57115	0.88767	0.57460
Numerical	0.00161	0.01188	0.08758	0.57152	0.88836	0.57534

demonstrates that there is ignored reflection when the wave travels through the artificial boundaries.

Example 2. In this example, we consider two different initial conditions:

$$\psi^{(0)}(x) = A_1 \mathrm{sech}[B(x + x_0)],$$

$$\phi^{(0)}(x) = A_2 \mathrm{sech}[B(x - x_0)],$$

$$\psi^{(1)}(x) = BvA_1 \mathrm{sech}[B(x + x_0)]\tanh[B(x + x_0)],$$

$$\phi^{(1)}(x) = -BvA_2 \mathrm{sech}[B(x - x_0)]\tanh[B(x - x_0)].$$

Figure 5 describes the numerical solution of CNLKGEs on the computational domain $[-15, 15]$. In Figs. 6(a) and 6(b), the energy and mass decay to zero as the wave passes through the boundaries, which shows the local ABCs can make the wave pass through the right and left boundaries well. Figure 6(c) shows how the reflection ratio changes over time. For comparison, a reference solution is solved in a larger interval $[-40, 40]$ and zero Dirichlet boundary conditions are imposed at $x = -40$ and $x = 40$. Table IV lists the corresponding numerical solutions and reference solutions at right artificial boundary for different times.

B. Two-dimensional examples

An exact solution of CNLKGEs in two dimensions is given in [1]:

$$\psi(x, y, t) = A_1 \mathrm{sech}[B_1 x + B_2 y - vt],$$

$$\phi(x, y, t) = A_2 \mathrm{sech}[B_1 x + B_2 y - vt],$$

where

$$A_1 = \sqrt{\frac{2a_1(c_1 - b_2)}{b_1 b_2 - c_1 c_2}}, \quad A_2 = \sqrt{\frac{2a_1(b_1 - c_2)}{c_1 c_2 - b_1 b_2}},$$

$$B_1 = \sqrt{\frac{-a_1}{v^2 - 2a^2}}, \quad B_2 = \sqrt{\frac{-a_2}{v^2 - 2a^2}}.$$

In order to test the accuracy of the numerical solution, the L_1, L_2, L_∞ errors are defined as similar as the one-dimensional case,

$$L_1\text{-E} = \frac{\sum_{j=0}^{J} \sum_{k=0}^{K} \left[\left|\psi_{j,k}^n - {}_{\mathrm{ex}}\psi_{j,k}^n\right| + \left|\phi_{j,k}^n - {}_{\mathrm{ex}}\phi_{j,k}^n\right|\right]}{2(J+1)(K+1)},$$

$$L_2\text{-E} = \left[\frac{h^2}{2} \sum_{j=0}^{J} \sum_{k=0}^{K} \left(\left|\psi_{j,k}^n - {}_{\mathrm{ex}}\psi_{j,k}^n\right|^2 + \left|\phi_{j,k}^n - {}_{\mathrm{ex}}\phi_{j,k}^n\right|^2\right)\right]^{1/2},$$

$$L_\infty\text{-E} = \frac{\max\left\{\left|\psi_{j,k}^n - {}_{\mathrm{ex}}\psi_{j,k}^n\right|\right\} + \max\left\{\left|\phi_{j,k}^n - {}_{\mathrm{ex}}\phi_{j,k}^n\right|\right\}}{2},$$

where ${}_{\mathrm{ex}}\psi_{j,k}^n$ and ${}_{\mathrm{ex}}\phi_{j,k}^n$ are exact solutions of the ψ and ψ at the point (x_j, y_k, t_n), respectively.

Assuming that the initial value of the original problem is satisfied, the wave propagates from the artificial boundary to the outside of the finite domain, and no wave propagates from the outside to the inside of the finite domain.

Example 3. The initial conditions of the CNLKGEs are chosen as

$$\psi^{(0)}(x, y) = A_1 \mathrm{sech}[B_1 x + B_2 y - vt - c_0],$$

$$\phi^{(0)}(x, y) = A_2 \mathrm{sech}[B_1 x + B_2 y - vt - c_0],$$

$$\psi^{(1)}(x, y) = A_1 \mathrm{sech}[B_1 x + B_2 y - vt - c_0]$$
$$\times \tanh[B_1 x + B_2 y - vt - c_0],$$

$$\phi^{(1)}(x, y) = A_2 \mathrm{sech}[B_1 x + B_2 y - vt - c_0]$$
$$\times \tanh[B_1 x + B_2 y - vt - c_0].$$

The truncated computational domain is $[0, 5] \times [0, 5]$, and this grid space is equal, i.e., $(h_x = h_y = h)$. Table V lists the error and convergence order on $T = 0.5$. One can observe that the convergence is almost second order. Figures 7–10 show the propagation of waves on the computational domain $[0, 5] \times [0, 5]$. Figures 11(a) and 11(b) show the change of energy and mass with time in the two-dimensional case, which illustrates the local ABCs method is efficient, because the local ABCs can make the wave pass through all the boundaries without dramatic reflection. The reflection ratio is similar to the one-dimensional case, and Fig. 11(c) shows that the fluctuations can cross artificial boundaries very well. Table VI lists the corresponding numerical solutions and exact solutions at the northeast corner for different times.

V. CONCLUSION

In this paper, the efficient local ABCs for CNLKGEs by applying the ideas of the operator splitting approach and artificial boundary method are developed. The

TABLE V. L_1, L_∞, and L_2 errors and the corresponding convergence order with the parameters $a = 1$, $a_1 = 1$, $b_1 = -1$, $c_1 = 1$, $a_2 = 1$, $b_2 = -2$, $c_2 = 0.5$, $T = 0.5$, $\tau = h^2$.

Mesh	L_∞-E	Order	L_1-E	Order	L_2-E	Order
$h = \frac{1}{2}$	2.502×10^{-1}		2.820×10^{-2}		3.348×10^{-1}	
$h = \frac{1}{4}$	5.450×10^{-2}	2.199	6.500×10^{-3}	2.117	7.040×10^{-2}	2.249
$h = \frac{1}{8}$	1.300×10^{-2}	2.068	1.600×10^{-3}	2.022	1.600×10^{-2}	2.138
$h = \frac{1}{16}$	3.200×10^{-3}	2.023	4.173×10^{-4}	1.926	4.000×10^{-3}	2.000

TABLE VI. An exact solution and numerical solution on the northeast corner point for different times.

	$T = 0.5$	$T = 1$	$T = 1.5$	$T = 2$	$T = 2.5$	$T = 3$	$T = 3.5$
Exact	1.77262	1.29491	0.84981	0.53262	0.32834	0.20146	0.12346
Numerical	1.77362	1.29611	0.85019	0.53161	0.32614	0.19866	0.12068

original problem defined on an unbounded domain is reduced to an initial boundary value problem on a bounded domain, which can be efficiently solved by finite difference method. The numerical results show the accuracy and validity of the local ABCs. However, some related problems have not been solved, such as general CNLKGEs (more than three solitary waves), which will be studied in the future.

[1] T. Alagesan, Y. Chung, and K. Nakkeeran, Chaos, Solitons Fractals **21**, 879 (2004).

[2] G. Makhankov, Phys. Rep. **35**, 1 (1978).

[3] D. Duncan, SIAM J. Numer. Anal. **34**, 1742 (1997).

[4] Y. Tourigny, IMA J. Numer. Anal. **10**, 449 (1990).

[5] W. Bao, Y. Cai, and X. Zhao, SIAM J. Numer. Anal. **52**, 2488 (2014).

[6] B. Ji, Numer. Methods Partial Differ. Equations **35**, 1056 (2019).

[7] Z. Xu, X. Dong, and Y. Yuan, J. Comput. Appl. Math. **292**, 402 (2016).

[8] X. Dong, Numerical Algorithms **62**, 325 (2013).

[9] S. Jiang, L. Greengard, and S. Wang, Adv. Comput. Math. **41**, 529 (2015).

[10] J. Grote, SIAM J. Appl. Math. **55**, 280 (1995).

[11] C. Zheng, J. Comput. Phys. **215**, 552 (2006).

[12] Z. Teng, J. Comput. Phys. **190**, 398 (2003).

[13] H. Han and C. Zheng, J. Comput. Math. **21**, 15 (2003).

[14] X. Antoine, A. Arnold, C. Besse, M. Ehrhardt, and A. Schädle, Commun. Comput. Phys. **4**, 729 (2008).

[15] Q. Du, H. Han, J. Zhang, and C. Zheng, SIAM J. Sci. Comput. **40**, A1430 (2018).

[16] W. Kong and Z. Huang, Numer. Math. **145**, 345 (2020).

[17] C. Li, H. Wang, H. Yue, and S. Guo, Appl. Numer. Math. **173**, 395 (2022).

[18] L. Higdon, Math. Comput. **47**, 437 (1986).

[19] S. Ji, G. Pang, X. Antoine, and J. Zhang, J. Comput. Phys. **444**, 110575 (2021).

[20] H. Han and X. Wu, *Artificial Boundary Method* (Spring-Verlag and Tsinghua Unversity Press, Berlin Heidelberg and Beijing, 2013).

[21] Z. Xu and H. Han, J. Comput. Phys. **225**, 1577 (2007).

[22] J. Zhang, Z. Xu, and X. Wu, Phys. Rev. E **78**, 026709 (2008).

[23] J. Zhang, Z. Xu, and X. Wu, Phys. Rev. E **79**, 046711 (2009).

[24] H. Li, X. Wu, and J. Zhang, Phys. Rev. E **84**, 036707 (2011).

[25] H. Han and Z. Zhang, J. Comput. Phys. **227**, 8992 (2008).

[26] H. Han and Z. Zhang, Commun. Comput. Phys. **10**, 1161 (2011).

[27] H. Han and Z. Zhang, J. Comput. Phys. **230**, 1319 (2011).

[28] S. Zhou and X. Cheng, Math. Comput. Simulat. **80**, 2362 (2010).

[29] H. Li and Y. Guo, Phys. Rev. E **96**, 063305 (2017).

[30] H. Li and Y. Guo, Appl. Math. Lett. **104**, 106286 (2020).